Syngas production from dry methane reforming over yttrium-promoted nickel- KIT-6 catalysts

Katarzyna Świrk, Maria Elena Gálvez, Monika Motak, Teresa Grzybek, Magnus Rønning, Patrick da Costa

▶ **To cite this version:**

HAL Id: hal-02308655

https://hal.sorbonne-universite.fr/hal-02308655v1

Submitted on 8 Oct 2019

Syngas production from dry methane reforming over yttrium-promoted nickel-KIT-6 catalysts

Katarzyna Świrk[1,2*], Maria Elena Gálvez[1], Monika Motak[2], Teresa Grzybek[2],

Magnus Rønning[3], Patrick Da Costa[1]

[1]Sorbonne Université, Institut Jean Le Rond d'Alembert,

Saint-Cyr l'Ecole F-78210, France

[2]AGH University of Science and Technology, Faculty of Energy and Fuels,

Cracow 30-059, Poland

[3]Norwegian University of Science and Technology, Department of Chemical Engineering,

Trondheim N-7491, Norway

*Corresponding author:

Katarzyna Świrk, swirk@agh.edu.pl

Sorbonne Université, Institut Jean Le Rond d'Alembert, Saint-Cyr l'Ecole F-78210, France

Abstract

Dry reforming of methane was studied over Ni,Y-promoted KIT-6 ordered mesoporous silicas, prepared by incipient impregnation (nickel content 12 wt.%, yttrium content of 4 wt.%, 8 wt.% or 12 wt.%). The catalysts were characterized by XRF, FT-IR, TGA/DSC-MS, N_2-adsorption, TEM, HRTEM, XRD and TPR-H_2. The promotion with 8 wt.% Y (Y/Si=0.05) resulted in the highest activity and H_2/CO molar ratio closer to the stoichiometric value at temperatures from 600 to 750°C. The characterization results of the yttrium promoted materials showed higher reducibility of the bulk NiO, bigger Ni crystallite size after reduction and DRM test, and better dispersion of nickel in the channels of the KIT-6 support. Additionally, larger Ni particles were observed on the external surface of the support, which may be related to catalytic selectivity towards carbon forming reactions. Upon dry methane reforming the segregated phases of Ni^o, Y_2O_3, and possibly $Y_2Si_2O_7$ were registered. No presence of a Ni,Y alloy was observed.

Keywords: KIT-6, nickel, yttrium, dry methane reforming

1. Introduction

Nowadays, fossil fuels are used as major energy sources. However, coal, natural gas and oil combustion results in greenhouse gas emissions, which, once released into the atmosphere, may cause important hazards to earth climate and human health. Carbon dioxide, one of the main components of exhaust gases, can be however utilized as raw material through different chemical processes, such as dry reforming of methane (DRM) [1]. In DRM, CO_2 reacts with CH_4, yielding synthesis gas (mixture of H_2 and CO) as final product [1–3]. The lack of selective and stable catalysts for DRM, together with the high endothermicity of this reaction, are the main obstacles for the scale-up and commercialization of this chemical CO_2 utilization process. Further catalyst development is therefore needed.

Nickel-based catalysts have been extensively studied in the last years [4–7]. Nickel is more readily available, active and relatively inexpensive compared to noble metals, i.e. Pt, Pd, Ru, Rh and Ir [7]. Active phase sintering and coking due to the simultaneous occurrence of carbon forming reactions are the main two drawbacks of nickel catalysts [8,9]. However, the choice of a proper support may inhibit these processes, through improved textural properties and enhanced dispersion of the active phase, leading to controlled selectivity and higher stability.

A wide variety of metal oxides, such as Al_2O_3, MgO, CeO_2, ZrO_2 or SiO_2, have been used as supports in the preparation of Ni-catalysts for DRM. Alumina shows excellent textural properties. Moreover, in Ni/Al_2O_3 catalyst a spinel phase ($NiAl_2O_4$) can be sometimes formed, which can considerably hinder carbon formation. However, as reported by Becerra *et al.* [10], the formation of this $NiAl_2O_3$ phase may lead to low catalytic activity, especially at relatively low temperatures. MgO is a support with high Lewis basicity. Therefore, Ni/MgO catalysts are particularly able to adsorb CO_2 molecules on their surface. Nevertheless, the activation of side reactions, such as reverse water-gas shift is very likely on this kind of materials [11–13]. Additionally, $Ni/MgO-Al_2O_3$ catalysts show good catalytic behavior. Modification with 20 wt.% of nickel was positive in terms of catalytic

activity, although enhanced formation of carbon deposit was reported [14]. The possible reason of the latter may be the inferior Ni dispersion, while modifying the support with high content of this metal. Furthermore, $MgAl_2O_4$ spinel may be also considered as a support. Alvar and Rezaei [15] examined this mesoporous material, subsequently modified with nickel, in dry reforming of methane. The catalyst showed high specific surface area and nanocrystalline structure, which benefited in catalytic activity, as well as in stability tests of DRM (no deactivation after 50 h). CeO_2 is known to have high oxygen storage capacity. Its use as support in the preparation of Ni-catalysts for DRM can lead to improved stability through the participation of labile oxygen in the oxidation of the carbon formed during DRM [16]. Asami *et al.* [17] reported almost negligible deactivation of a Ni/CeO_2 catalyst during DRM at 850ºC. At lower reaction temperatures, i.e. 700ºC, a decrease in stability was however registered. Moreover, cerium may be used as promoter in DRM process. As studied by Dębek *et al.* [18] the addition of this metal to Ni-based Mg,Al-mixed oxides derived from hydrotalcites resulted in better activity compared to non-promoted material. This contributed to enhanced reducibility by introduction of new oxygen pairs. The authors also tested Zr-promoted hydrotalcite catalysts [18]. The addition of zirconium significantly improved stability in the DRM test at 550°C, since it inhibited the reaction of direct methane decomposition. Moreover, modification with both, Ce and Zr, resulted in better stability and, in the same time, decreased catalytic activity. This could be ascribed to higher amount of basic sites with strong strength [19]. Zirconium oxides are also used as carriers for DRM due to their appropriate basicity and weak acid properties. As studied by Rezaei *et al.* [20] zirconia supports promoted with K_2O showed improved catalytic activity and stability, which was due to enhanced basicity in the materials. Moreover, Tunisian natural clays also may find their application as supports in CO_2 reforming reaction. Liu *et al.* [21] examined the influence of ceria and zirconia promotion (added separately) on Cu-pillared and Fe-pillared clays. The modification with metal oxides increased the number of medium and weak basic sites, together with Niº crystalline size, which resulted in increased catalytic activity during DRM test, and a presence of carbon forming reactions. Silica mesoporous materials are also considered attractive

carriers due to their high specific surface area, mesopore-enriched porosity and good thermal stability [22]. Huang *et al.* [22] studied SiO_2 supports loaded with Ni. The use of SiO_2 allowed to obtain very high dispersion of the Ni-phase and controlled crystallite sizes, leading to improved catalytic performance. Lovell *et al.* [23] studied SiO_2 supports, which were prepared through flame spray pyrolysis and subsequently loaded with nickel. The best catalytic performance in DRM was registered for the catalysts having the highest surface area and showing the smallest Ni crystallite size of the series. Recently, considerable attention has also been paid to the ordered mesoporous silica SBA-15. Gálvez *et al.* [24] studied Ni/SBA-15 catalysts, which were synthesized by three different ways (impregnation, co-precipitation and co-precipitation with ascorbic acid). The pre-reduction of the Ni-phase using ascorbic acid resulted in a very accurate control of Ni-crystallite size, leading to Ni-particles placed inside the mesopores of the SBA-15 structure, resulting in enhanced activity, selectivity and stability.

Promotion with different metals can also positively influence catalytic behavior of DRM catalyst. Samarium-promoted Ni-SBA-15 catalysts were tested in DRM by Taherian *et al.* [25]. The promotion with Sm resulted in enhanced stability and catalytic activity due to the increase in dispersion of NiO and its better interaction with SBA-15. Erdogan *et al.* [26] examined the effect of nickel and cobalt addition into SBA-15 support. The formation of Ni-Co alloy hindered agglomeration of nickel particles, resulting in suppressed carbon deposit formation. Kaydouh *et al.* [27] studied SBA-15 loaded with Ni and Ce, which were highly active and stable in DRM. However, the promoting effect of Ce was not clear, since no significant differences in terms of Ni-reducibility and catalytic activity were observed for the Ce-promoted and the non-promoted catalysts. Albarazi *et al.* [28,29] examined the DRM activity of Ni/SBA-15 catalysts modified with $Ce_{0.75}Zr_{0.25}O_2$. The presence of Ce and Zr promoters resulted in higher catalytic activity, i.e. higher CH_4 conversions, and improved stability in the low temperature range (600-630°C). B. Li *et al.* [30] prepared Ni,Y-modified SBA-15. The authors reported that yttrium caused a decrease in Ni° size, linked to enhanced reducibility of the Ni-phase in the calcined catalyst. This was related with an increased number of oxygen vacancies. J.F.

Li *et al.* [8] also reported a positive effect of Y-promotion of Ni/SBA-15 catalysts. The authors prepared different catalysts using 6, 3 and 9 wt.% yttrium loading, for a fixed amount of nickel (9 wt.%). The 9%Y-Ni/SBA-15 catalyst evidenced the lowest carbon formation and the highest catalytic activity of the series.

Due to its high specific surface area and very particular pore size distribution, KIT-6 ordered mesoporous silica with Ia3d symmetric structure has been recently considered as support in the preparation of catalysts for various processes [31–39]. For example, Ni-KIT-6 were examined in pyrolysis of cellulose [39], Ni-La/KIT-6 catalysts were tested in CO_2 reforming [38]; Ni-V/KIT-6, Ni-Ce/KIT-6, Ni-La/KIT-6 and Ni-Mn/KIT-6 in CO methanation [33]; Cu/KIT-6 for thiophene removal [35]; SO_4^{2-}/Zr-KIT-6 for esterification of oleic acid [31]; and Ti/KIT-6 for epoxidation of cyclohexene [32]. However, to the best of our knowledge there are no studies reporting the use of yttrium as promoter on Ni-containing KIT-6 supported catalysts for dry reforming applications.

Thus, the aim of the present study was to prepare Ni,Y-modified KIT-6 catalysts and evaluate their activity and selectivity in dry reforming of methane. Catalysts with different Y loadings were thus prepared, characterized and tested in DRM at moderate temperature, i.e. 600-750°C. The fresh, calcined, reduced and spent catalysts were characterized by means of X-ray fluorescence (XRF), Fourier transformed infrared spectroscopy (FT-IR), thermal gravimetric analysis/ differential scanning calorimetry-mass spectrometry (TGA/DSC-MS), N_2 adsorption-desorption analysis, transmission electron microscopy (TEM), high-resolution transmission electron microscopy (HRTEM), X-ray diffraction (XRD), and hydrogen temperature-programmed reduction (TPR-H_2).

2. Experimental

2.1. Catalyst preparation

The mesoporous KIT-6 material was synthesized as described elsewhere [34]. In short, 7.47 g of aqueous solution of HCl (37%) was dissolved in 144 cm^3 of distilled water. Then 4 g of P123 triblock polymer were added and the solution was stirred for 4h. Afterwards, the temperature of solution was

increased to 35ºC and butanol (4g) was added dropwise. The solution was stirred for another 1h. Finally, TEOS (Tetraethyl orthosilicate, 8.6 g) was introduced while stirring at 35ºC. After 24h, the mixture was transposed into a Teflon bottle for hydrothermal synthesis. The synthesis was carried out under static conditions at 90ºC for 24h. The obtained product was filtered and dried at 100ºC overnight. In order to remove the template, calcination was performed at 600ºC for 6h.

Incipient wetness impregnation was used to prepare the KIT-6 supported Ni-Y catalysts. A mixture of aqueous solutions of $Ni(NO_3)_2 \cdot 6H_2O$ and $Y(NO_3)_3 \cdot 6H_2O$ was used as precursors in order to achieve the fixed amount of nickel (12 wt.%), and different content of yttrium in each sample (4 wt.%, 8 wt.% or 12 wt.%, respectively). After the impregnation, the samples were dried overnight and then calcined in air at 550ºC for 5 h in order to remove the nitrates and to form NiO on the catalyst as described elsewhere [18].

2.2. Catalysts characterization

XRF (Supermini200) was performed to determine the elemental composition of the catalysts. The measurements were carried out under vacuum at 36.5ºC. A proportional counter detector (PC) was used under P-10 gas (mixture of 10% CH_4/Ar) with flow of 24.7 cm^3/min. The samples were diluted in boric acid with a ratio of 1:200, and then pelletized under pressure of 10 bar. Just before tests the samples were covered with 6μm polypropylene film. FT-IR spectra were obtained in a Fourier-transform infrared spectrometer Thermo Nicolet 380, in the range of 4000 to 400 cm^{-1}. The samples were pelletized together with KBr at the ratio of 1:100. TGA/DSC-MS experiments were performed in a Netzsch STA 449C Jupiter TGA/DSC and NetzschAëlos QMS 403 MS. For this purpose, 8 mg of fresh sample was used to measure weight loss, DSC signal and current as a function of temperature (from room temperature to 800ºC). The tests were performed in air using a total flow of 100 ml/min. The products analyzed by mass spectrometry were m/e= 44 (CO_2 or N_2O) and 18 (H_2O). TEM analyses were performed in JOEL JEM-100XCII microscope. HRTEM analysis was carried out in a JEM-2100Plus Transmission Electron Microscope. N_2 adsorption-desorption isotherms were

acquired with the help of a Micromeritics TriStar II device at -195°C. Prior to analysis, the samples were outgassed at 300°C for 3 h [35]. Specific surface area and pore diameters were respectively calculated using the Brunauer-Emmett-Teller (BET) and Barrett-Joyner-Halenda (BJH) method. XRD patterns were recorded by a PANalytical-Empyrean diffractometer equipped with a Cu Kα (λ=0.15406 nm) radiation source. The measurements were carried out in the 2Θ range of 3 to 90°. Temperature-programmed reduction (TPR-H$_2$) measurements were performed in a BEL Japan BELCAT-M apparatus, equipped with a TCD detector. Typically, 60 mg of each catalyst was first degassed in helium at 100°C for 2 h, and then reduced in the mixture of 5 % H$_2$/Ar at temperature range from 100°C to 750°C (heating rate of 7.5°C/min).

2.3. DRM catalytic activity

Dry reforming of methane tests were carried out at atmospheric pressure in a fixed bed quartz reactor with a thermocouple type K in contact with the catalytic bed and protected by a quartz shield. Before reaction, all the catalysts were reduced in situ at 750°C for 1h in a mixture of 5% H$_2$/Ar (heat rate 10°C/min) in order to have all the nickel particles reduced (Ni°) [33]. The catalytic activity was evaluated in the temperature range of 750-600°C with a temperature step every 50°C, and 0.5 h step at each temperature to obtain steady state. In order to check initial stability of the catalysts, additional DRM tests were carried out for 5 hours at 700°C. In both types of experiments, the total flow was 100 cm^3/min and the composition of the inlet gas mixture was CH$_4$/CO$_2$/Ar=1/1/8 (GHSV=20,000 h^{-1}). The outlet gases were analyzed by gas chromatograph (490 Varian Micro-GC).

The respective conversions of CH$_4$, CO$_2$, and H$_2$/CO molar ratio where calculated as follows:

$$CH_{4\,conversion}[\%] = \frac{n_{CH_4,initial} - n_{CH_4,final}}{n_{CH_4,initial}} \cdot 100, \tag{1}$$

$$CO_{2\,conversion}[\%] = \frac{n_{CO_2,initial} - n_{CO_2,final}}{n_{CO_2,initial}} \cdot 100, \tag{2}$$

$$H_2 / CO = \frac{n_{H_2, final}}{n_{CO, final}}, \tag{3}$$

Where $n_{CH4, initial}$ and $n_{CO2, initial}$ are the inlet numbers of moles of methane and carbon dioxide, respectively. And $n_{CH4, final}$, $n_{CO2, final}$, $n_{H2, final}$, $n_{CO, final}$ are outlet number of moles of methane, carbon dioxide, hydrogen and carbon oxide, respectively.

3. Results and discussion

3.1. Catalyst characterization

3.1.1. Textural and structural properties

The composition of the different KIT-6 supported catalysts is given in Table 1. Silicon is the main component with a content of ca. 90% in every sample. Nickel loading resulted Ni contents close to the nominal value, i.e. 12 wt.% vis-à-vis 7-10 wt.% measured in the catalysts after calcination. Only 50% of the nominal Y loading was found in the calcined catalysts. Final yttrium amounts are 2 wt.% to 7 wt.% in comparison to nominal loads ranging from 4 wt.% to 12 wt.%, respectively (Table 1).

The FT-IR spectra acquired for the different catalysts are presented in Fig. 1. The peaks observed at 464, 960, 807 and 1083 cm⁻¹ correspond to the bending vibration of Si-O-Si, the stretching vibrations of Si-OH, symmetric and asymmetric stretching vibrations of Si-O-Si, respectively. The mentioned vibrations are assigned to KIT-6, and related to the formation of condensed framework of silica. FT-IR analysis thus confirms the successful synthesis of KIT-6 material. In addition, the bands at 1640 and 3435 cm⁻¹ are due to the presence of absorbed water molecules, namely the stretching vibration of O-H [38]. The double peak at 2858 and 2978 cm⁻¹ can be ascribed to the P123 template [40,41]. This peak disappeared for Ni,Y-modified samples, as a consequence of the calcination of KIT-6 at 600ºC. The peak at 1380 cm⁻¹ can be ascribed either to the remaining presence of template molecules or to or the N-O vibration of the nitrates used in the impregnation [36]. Since this peak looks more intense for the Ni-Y modified catalysts, it can be therefore linked to the presence of

residues of the nitrates used in the impregnation. Its intensity decreases however with the addition of larger amounts of yttrium.

Fig. 2 shows TGA/DSC-MS curves acquired for the different materials prepared. The KIT-6 support is shown in Fig. 2A. Two main weight-loss regions can be observed: 4% between 50 and 200°C, and 37% from 200 to 600°C. The former corresponds to the removal of physically adsorbed water (m/e=18). The latter arises from water removal, and from the combustion/decomposition of synthesis residues (organic compounds, yielding CO_2 m/e = 44). Fig. 2B to E show the TGA curves obtained for the KIT-6 supported catalysts. The weight-loss measured increases with Y-loading. The peaks at 200, 300 and 600ºC can be ascribed to the evaporation of physisorbed water, to the removal of the water molecules present within the micropore walls and to silanol condensation, respectively [42]. MS analysis evidenced low current signals for m/e=44. Catalyst calcination resulted in the elimination of a considerable part of the KIT-6 synthesis residues, i.e. P123. However, a slight shoulder can still be observed at 300ºC and be attributed to N_2O evolution during thermal decomposition of nitrates.

TEM images of the calcined support are presented in Fig. 3. The characteristic la3d structure of KIT-6 can be clearly observed, further confirming the successful synthesis of this ordered mesoporous material [31–38]. Highly ordered mesopores create a bi-continuous network of channels. This structure is further confirmed at the sight of the obtained N_2-adsorption isotherms, as discussed later on. The pore size, measured by using ImageJ software, varies from 3.8 to 6.3 nm.

Fig. 4A shows N_2 adsorption-desorption isotherms for the modified KIT-6 supports. All catalysts revealed type IV isotherms with an H1 hysteresis loop, which is typical of such ordered mesostructured materials [34,38]. The maintained shape of the isotherms shows that the structure of the catalysts does not change after upon nickel and yttrium loading. The pore distribution was bimodal in all cases (Fig. 4B), revealing two types of pores (i) narrow pores (of ca. 3.5 nm) and (ii) wide pores (with mean diameter between 4.5 to 4.8 nm). The textural properties are summarized in Table 1. The

highest S_{BET} was obtained for KIT-6 support (456 m^2/g), and after further modification with Ni and Y the specific surface area and pore volumes decreased, as a consequence of pore blockage occurring to a certain extent upon metal loading.

XRD patterns for KIT-6 support of freshly prepared samples and after calcination at 600°C for 6h are presented in Fig. 5. The wide reflection at ca. 2Θ = 23° can be attributed to SiO$_2$ [33]. Fig. 6A shows the Y-promoted materials after calcination at 550°C. In all patterns the characteristic XRD reflection of amorphous silica (2Θ = 23°) and the reflections typical of NiO (2Θ = 37.3, 43.3, 63, 75.4, 79.4°) are observed. Additionally, a small shoulder at ca. 2Θ = 29° was registered. The presence of this shoulder can be linked to the existence of a segregated Y$_2$O$_3$ phase [30]. No shift towards higher Bragg angles has been detected in the XRD diffractograms, which may point to the absence of Ni-Y mixed phase.

3.1.2. Reducibility of KIT-6 based catalysts

Fig. 7 shows TPR-H$_2$ results for the synthesized KIT-6 materials. For the (Ni)/KIT-6 catalysts, three wide poorly resolved reduction peaks were observed at 373, 433 and 650°C. The first one is associated with reduction of NiO species weakly interacting with KIT-6 [33,39], the second refers to reduction of bulk NiO [33,37], while the third may be attributed to NiO located in the pores of the support [37]. As a consequence of yttrium addition, a shift towards higher reduction temperatures and the change in peaks shape can be clearly observed. Narrow peaks appear at around 418°C, their intensity increasing with increasing Y-loading. Table 2 presents H$_2$ consumption obtained for the reduction of bulk NiO (I type) and reduction of NiO located inside pores (type II) as calculated from Fig. 7. The reducibility of the bulk NiO increases with the addition of yttrium, whereas the opposite was observed for NiO located inside the pores. The values were decreasing with the yttrium loading, which may suggest that sintering is occurring with less of Ni° inside the pores. Moreover, the ratio between the H$_2$ consumption for NiO inside pores to the total consumption is decreasing for the

samples with yttrium. The yttrium promotion affects reducibility of nickel species, and all the tested catalysts could be reduced at 750ºC.

Only minor textural changes were found for the catalysts after TPR-H_2 tests, as proven by the N_2 adsorption-desorption experiments (Table 1). The shape of the isotherms and quantity adsorbed remained stable. The specific surface area was slightly lower for these samples, and there were no changes of pore volume and pore diameters.

Fig. 6B presents XRD patterns for the reduced materials. Apart from the SiO_2 reflection, and the one corresponding to Y_2O_3, the characteristic reflections of metallic nickel Niº ($2\Theta = 44.5, 52, 76.5º$) are also present. Additionally, by comparing diffractograms of the doubly promoted samples to the Y-free catalyst, no shift in the Niº reflections was observed. The Ni particle sizes calculated from the Scherrer equation are presented in Table 2. An increase in nickel crystallite size after reduction is generally observed, which becomes more evident for the Y-modified catalysts. The Niº crystallite size varies from 4 nm for non-promoted catalyst (Ni)/KIT-6 to 13 nm for the highest Y-loading catalyst (Ni-12Y)/KIT-6.

TEM images for the reduced catalysts are shown in Fig. 8. Compared to the micrographs of the unmodified KIT-6 support (Fig. 3), it can be concluded that the ordered silica mesoporous structures were well preserved and that metallic Ni particles were present, which is in accordance with the results obtained by XRD (Fig. 6B). Two populations of Niº particles can be observed, one inside the channel and another outside the mesoporous structure. The average particle size inside the pores, measured by ImageJ software, was 14 nm and 9 nm for (Ni)/KIT-6 and (Ni-8Y)/KIT-6, respectively. For the Y-modified sample nickel particles are better dispersed in the channels of the KIT-6 support than for in (Ni)/KIT-6 catalyst, where the particles are present only in some spots of KIT-6 support.

3.2. Catalytic activity in dry reforming of methane

Fig. 9A to C present results of catalytic tests over KIT-6 modified catalysts. The increase of activity with the increasing temperature may be observed. The DRM activity follows the sequence: KIT-6 < (Ni-12Y)/KIT-6 < (Ni-4Y)/KIT-6 < (Ni)/KIT-6 < (Ni-8Y)/KIT-6, confirming that Y-promotion significantly improves catalytic behavior of the prepared catalysts. The best results for both CH_4 and CO_2 conversions were obtained for the catalyst containing 8 wt.% of yttrium, corresponding to Y/Si ratio of 0.05 in the tested temperature range.

The positive role of yttrium has already been reported in the literature. J.F. Li *et al.* [8] observed that 9 wt.% yttrium promotion of a SBA-15 catalyst led to the highest conversion among the tested catalysts with yttrium loading varying from 3 wt.% and 9 wt.%. This observation was explained by the positive influence of yttrium on Ni dispersion. B. Li *et al.* [30] also reported that surface oxygen vacancies are initiated from yttrium incorporation into SBA-15, which activated the sites and endorsed CH_4 and CO_2 conversion. The optimal ratio for Y/Si was found to be 0.04. Y/Si molar ratio of 0.08 resulted in the destruction of the mesoporous structure of the support, hindering the catalytic activity. Similar conclusions can be derived from Fig. 9. At 750°C the maximum CH_4 and CO_2 conversions are 66.1 and 72.3%, respectively. The H_2/CO molar ratio is presented in Fig. 9C. The obtained values are lower than unity, which suggests the occurrence of side reactions. More carbon oxide (CO) was formed than hydrogen (H_2) and the highest values were observed for (Ni-8Y)/KIT-6 (Y/Si=0.05) which is in agreement with the literature [30]. Moreover, higher CO_2 conversions with respect to CH_4 were also reported and ascribed to the presence of parallel reactions, such as reverse water-gas shift [8].

The stability tests were carried out for the two best performing samples, i.e. (Ni)/KIT-6 and (Ni-8Y)/KIT-6. The amount of formed carbon, calculated from C balance in an isothermal 5-hour test at 700°C, was 0.663 and 0.367 mg_C/g_{cat}·h for Ni/KIT-6 and Ni-8Y/KIT-6, respectively, by obtaining the CH_4 conversion of 46.7 % and 51.4 %. The introduction of Y resulted in a lower amount of deposited

carbon at tested temperature. Dębek *et al.* [43] observed clear correlation between nickel particle size and formed carbon. The relatively small Ni particles hinder the carbon forming reaction, i.e. direct methane decomposition ($CH_4 = C + 2H_2$). This reaction is favorable at relatively low temperature, at 550ºC [43]. Thus, the values obtained from the carbon balance (at 700ºC) may not directly relate to the presence of methane decomposition in Y-promoted sample, which will be further discussed.

3.3. Characterization of the spent catalysts

3.3.1. Textural and structural properties

Fig. 10 shows TEM images of (A) KIT-6 support, (B) (Ni)/KIT-6, and (C) (Ni-8Y)/KIT-6 after DRM activity tests. No significant changes occurred after the experiment on KIT-6 material, which suggests that the synthesized support is resistant to DRM conditions. On the other hand, graphitic filament carbon was formed in all the catalysts, and it arises from the methane decomposition reaction, and possibly from CO disproponation ($2CO = CO_2 + C$) [8]. The former is strongly dependent on the size of Ni particles, and it is favored at low-temperature DRM. The nickel particles observed in the micrographs are predominantly located in the channels of KIT-6, and additionally on the external surface of the carrier. KIT-6 promoted with yttrium clearly shows better dispersion of nickel in the channels, although additionally larger nickel particles were observed on the external surface of the support. The latter is responsible for the formation of surface carbon [8], and as presented in TEM images, greater amount was observed in spent (Ni-8Y)/KIT-6 catalyst. Table 2 summarizes the average particle size inside the pores for (Ni)/KIT-6 and (Ni-8Y)/KIT-6 spent catalysts, i.e. 11 nm and 8 nm, respecively. The average size of larger particles, located on external surface, was 26 nm and 51 nm for (Ni)/KIT-6 and (Ni-8Y)/KIT-6, respectively. Thus, the yttrium promotion improves dispersion of small Ni° particles located inside pores of the support. However, in case of Ni° particles on the external surface, the particles are bigger for Y-promoted catalysts compared to the un-promoted one. The latter may be the reason of the higher amount of carbon formed on (Ni-8Y)/KIT-6 during the reaction, as confirmed by TEM images (Fig. 10) and in agreement with

the literature [8]. HRTEM is presented in Fig. 11 for (Ni-8Y)/KIT-6 sample. Metallic nickel, plane (111) with d-spacing of 1.98Å is observed. No yttrium was detected in this image, which is in good agreement with XRD results (separate phase of Ni°). Also, well distributed particles of Ni° are shown in Fig. 11B. The particles may be located inside the channels, or on the surface of the KIT-6 support. Fig. 11C shows a Y_2O_3 with an intereticular distance d_{hkl} equal to 3.06 Å corresponding to a (222) plane. No presence of nickel was registered in the micrograph, which shows no interaction between these two metals in the catalyst. The Y_2O_3 was observed before in SBA-15 modified samples in the studies of B. Li *et al.* [30] and J. F. Li *et al.* [8]. However, the obtained value may also arise from (021) plane of monolitic $Y_2Si_2O_7$ (d_{hkl}=3.05 Å).

Fig. 12 presents XRD patterns of the samples after DRM. In comparison to the diffractograms shown in Fig. 6B, reflections at 2Ɵ ca. 27° appeared. They may be assigned to graphitic carbon. The average Ni° crystallite sizes calculated from Scherrer equation (Table 2) are 5 nm, 9 nm, 18 nm, and 23 nm for (Ni)/KIT-6, (Ni-4Y)/KIT-6, (Ni-8Y)/KIT-6, and (Ni-12Y)/KIT-6, respectively. These values are higher compared to the crystal size calculated for reduced samples. A possible reason may be the formation of nickel agglomerates on the outer surface, due to increasing loading of yttrium. This is consistent with the TEM results. Bigger Ni° crystal size increases activity towards direct methane decomposition. However, the values obtained for the Y promoted sample are not in agreement with the calculated carbon balance from the initial stability test at 700°C, indicating that the other dominant reaction at this specific temperature is occurring rather than carbon formation.

4. Conclusions

KIT-6 ordered mesoporous silica with Ia3d symmetric structure was synthesized and modified with nickel and yttrium. (Ni-8Y)/KIT-6, corresponding to Y/Si=0.05, presented the highest activity in dry methane reforming at temperatures from 600 to 750°C, compared to (Ni)/KIT-6, (Ni-4Y)/KIT-6 and (Ni-12Y)/KIT-6. The prepared catalysts showed characteristic absorption spectra for silica material, larger Ni crystallite size, and higher reducibility of bulk NiO for Y-promoted materials than

(Ni)/KIT-6. TEM analysis of reduced and spent catalysts revealed the stable structure of the support. For promoted catalysts, TEM images showed incorporation of metallic nickel into the channels of the support, as well as presence of larger Ni particles on the external surface. For the former, better dispersion was observed in the sample promoted with nickel and yttrium as compared to the sample only modified with nickel. For the latter, nickel agglomerates are present on the outer surface, and they contribute to a higher extent of filamentous carbon formation on Y-modified catalysts compared to catalysts without addition of Y. HRTEM analysis showed no presence of Ni,Y alloy formation in spent catalysts. Additionally, separate phases of Ni^o, Y_2O_3, and possibly $Y_2Si_2O_7$ were observed.

Acknowledgements

References

[1]   Aresta M, Dibenedetto A. Utilisation of CO_2 as a chemical feedstock: opportunities and challenges. Dalt Trans 2007:2975–92. doi:10.1039/b700658f.

[2]   Wang N, Yu X, Shen K, Chu W, Qian W. Synthesis, characterization and catalytic performance of MgO-coated Ni/SBA-15 catalysts for methane dry reforming to syngas and hydrogen. Int J Hydrogen Energy 2013;38:9718–31. doi:10.1016/j.ijhydene.2013.05.097.

[3]   Zhang L, Li L, Zhang Y, Zhao Y, Li J. Nickel catalysts supported on MgO with different specific surface area for carbon dioxide reforming of methane. J Energy Chem 2014;23:66–72. doi:10.1016/S2095-4956(14)60119-4.

[4]   Kawi S, Kathiraser Y, Ni J, Oemar U, Li Z, Saw ET. Progress in Synthesis of Highly Active and Stable Nickel-Based Catalysts for Carbon Dioxide Reforming of Methane. ChemSusChem 2015;8:3556–75. doi:10.1002/cssc.201500390.

[5]   Hu YH, Ruckenstein E. The characterization of a highly effective NiO/MgO solid solution catalyst in the CO_2 reforming of CH_4. Catal Letters 1997;43:71–7. doi:10.1023/A:1018982304573.

[6]   Min J-E, Lee Y-J, Park H-G, Zhang C, Jun K-W. Carbon dioxide reforming of methane on Ni–MgO–Al_2O_3 catalysts prepared by sol–gel method: Effects of Mg/Al ratios. J Ind Eng Chem 2015;26:375–83. doi:http://dx.doi.org/10.1016/j.jiec.2014.12.012.

[7]   Fan MS, Abdullah AZ, Bhatia S. Utilization of greenhouse gases through dry reforming: Screening of nickel-based bimetallic catalysts and kinetic studies. ChemSusChem 2011;4:1643–53. doi:10.1002/cssc.201100113.

[8]   Li JF, Xia C, Au CT, Liu BS. Y_2O_3-promoted NiO/SBA-15 catalysts highly active for CO_2/CH_4 reforming. Int J Hydrogen Energy 2014;39:10927–40. doi:10.1016/j.ijhydene.2014.05.021.

[9]   Zhang J, Wang H, Dalai AK. Development of stable bimetallic catalysts for carbon dioxide

reforming of methane. J Catal 2007;249:300–10. doi:10.1016/j.jcat.2007.05.004.

[10]   Becerra A, Dimitrijewits M, Arciprete C, Luna AC. Stable Ni/Al$_2$O$_3$ catalysts for methane

dry reforming Effects of pretreatment. Granul Matter 2001;3:79–81.

[11]   Zanganeh R, Rezaei M, Zamaniyan A. Dry reforming of methane to synthesis gas on NiO-

MgO nanocrystalline solid solution catalysts. Int J Hydrogen Energy 2013;38:3012–8.

doi:10.1016/j.ijhydene.2012.12.089.

[12]   Zanganeh R, Rezaei M, Zamaniyan A. Preparation of nanocrystalline NiO-MgO solid

solution powders as catalyst for methane reforming with carbon dioxide: Effect of

preparation conditions. Adv Powder Technol 2014;25:1111–7.

doi:10.1016/j.apt.2014.02.015.

[13]   Jafarbegloo M, Tarlani A, Mesbah AW, Sahebdelfar S. One-pot synthesis of NiO–MgO

nanocatalysts for CO$_2$ reforming of methane: The influence of active metal content on

catalytic performance. J Nat Gas Sci Eng 2015;27:1165–73.

doi:10.1016/j.jngse.2015.09.065.

[14]   Alipour Z, Rezaei M, Meshkani F. Effect of Ni loadings on the activity and coke formation

of MgO-modified Ni/Al$_2$O$_3$ nanocatalyst in dry reforming of methane. J Energy Chem

2014;23:633–8. doi:10.1016/S2095-4956(14)60194-7.

[15]   Alvar EN, Rezaei M. Mesoporous nanocrystalline MgAl$_2$O$_4$ spinel and its applications as

support for Ni catalyst in dry reforming. Scr Mater 2009;61:212–5.

doi:10.1016/j.scriptamat.2009.03.047.

[16]   Odedairo T, Chen J, Zhu Z. Metal-support interface of a novel Ni-CeO$_2$ catalyst for dry

reforming of methane. Catal Commun 2013;31:25–31. doi:10.1016/j.catcom.2012.11.008.

[17]   Asami K, Li X, Fujimoto K, Koyama Y, Sakurama A, Kometani N., Yonezawa Y. CO$_2$

reforming of CH4 over ceria-supported metal catalysts. Catal Today 2003;84:27–31.

doi:10.1016/S0920-5861(03)00297-9.

[18]   Dębek R, Galvez ME, Launay F, Motak M, Grzybek T, Da Costa P. Low temperature dry methane reforming over Ce, Zr and CeZr promoted Ni–Mg–Al hydrotalcite-derived catalysts. Int J Hydrogen Energy 2016;41:11616–23. doi:10.1016/j.ijhydene.2016.02.074.

[19]   Dębek R, Motak M, Galvez ME, Grzybek T, Da Costa P. Influence of Ce/Zr molar ratio on catalytic performance of hydrotalcite-derived catalysts at low temperature CO_2 methane reforming. Int J Hydrogen Energy 2017;42:1–12. doi:10.1016/j.ijhydene.2016.12.121.

[20]   Rezaei M, Alavi SM, Sahebdelfar S, Yan Z. Effects of K_2O Promoter on the Activity and Stability of Nickel Catalysts Supported on Mesoporous Nanocrystalline Zirconia in CH4 Reforming with CO2. Energy & Fuels 2008;22:2195–202. doi:10.1016/S1003-9953(08)60064-X.

[21]   Liu H, Da Costa P, Hadj Taief HB, Benzina M, Gálvez ME. Ceria and zirconia modified natural clay based nickel catalysts for dry reforming of methane. Int J Hydrogen Energy 2017;42:23508–16. doi:10.1016/j.ijhydene.2017.01.075.

[22]   Huang F, Wang R, Yang C, Driss H, Chu W, Zhang H. Catalytic performances of Ni/mesoporous SiO_2 catalysts for dry reforming of methane to hydrogen. J Energy Chem 2016;25:709–19. doi:10.1016/j.jechem.2016.03.004.

[23]   Lovell E, Scott J, Amal R. Ni-SiO_2 Catalysts for the Carbon Dioxide Reforming of Methane: Varying Support Properties by Flame Spray Pyrolysis. Molecules 2015;20:4594–609. doi:10.3390/molecules20034594.

[24]   Gálvez ME, Albarazi A, Da Costa P. Enhanced catalytic stability through non-conventional synthesis of Ni/SBA-15 for methane dry reforming at low temperatures. Appl Catal A Gen 2015;504:143–50. doi:10.1016/j.apcata.2014.10.026.

[25]   Taherian Z, Yousefpour M, Tajally M, Khoshandam B. Promotional effect of samarium on the activity and stability of Ni-SBA-15 catalysts in dry reforming of methane. Microporous Mesoporous Mater 2017;251:9–18. doi:10.1016/j.micromeso.2017.05.027.

[26] Erdogan B, Arbag H, Yasyerli N. SBA-15 supported mesoporous Ni and Co catalysts with high coke resistance for dry reforming of methane. Int J Hydrogen Energy 2018;43:1396–405. doi:10.1016/j.ijhydene.2017.11.127.

[27] Kaydouh MN, El Hassan N, Davidson A, Casale S, El Zakhem H, Massiani P. Highly active and stable Ni/SBA-15 catalysts prepared by a "two solvents" method for dry reforming of methane. Microporous Mesoporous Mater 2016;220:99–109. doi:10.1016/j.micromeso.2015.08.034.

[28] Albarazi A, Gálvez ME, Da Costa P. Synthesis strategies of ceria-zirconia doped Ni/SBA-15 catalysts for methane dry reforming. Catal Commun 2015;59:108–12. doi:10.1016/j.catcom.2014.09.050.

[29] Albarazi A, Beaunier P, Da Costa P. Hydrogen and syngas production by methane dry reforming on SBA-15 supported nickel catalysts: On the effect of promotion by $Ce_{0.75}Zr_{0.25}O_2$ mixed oxide. Int J Hydrogen Energy 2013;38:127–39. doi:10.1016/j.ijhydene.2012.10.063.

[30] Li B, Zhang S. Methane reforming with CO_2 using nickel catalysts supported on yttria-doped SBA-15 mesoporous materials via sol-gel process. Int J Hydrogen Energy 2013;38:14250–60. doi:10.1016/j.ijhydene.2013.08.105.

[31] Gopinath S, Kumar PSM, Arafath KAY, Thiruvengadaravi K V., Sivanesan S, Baskaralingam P. Efficient mesoporous SO_4^{2-}/Zr-KIT-6 solid acid catalyst for green diesel production from esterification of oleic acid. Fuel 2017;203:488–500. doi:10.1016/j.fuel.2017.04.090.

[32] Kumaresan L, Prabhu A, Palanichamy M, Murugesan V. Mesoporous Ti-KIT-6 molecular sieves: Their catalytic activity in the epoxidation of cyclohexene. J Taiwan Inst Chem Eng 2010;41:670–5. doi:10.1016/j.jtice.2010.02.004.

[33] Cao HX, Zhang J, Guo CL, Chen JG, Ren XK. Highly dispersed Ni nanoparticles on 3D-

mesoporous KIT-6 for CO methanation: Effect of promoter species on catalytic performance. Cuihua Xuebao/Chinese J Catal 2017;38:1127–37. doi:10.1016/S1872-2067(17)62862-6.

[34] Pirez C, Caderon J, Dacquin J, Lee AF, Wilson K. Tunable KIT-6 Mesoporous Sulfonic Acid Catalysts for Fatty Acid Esteri fi cation. ACS Catal 2012:2–7. doi:10.1021/cs300161a.

[35] Subhan F, Aslam S, Yan Z, Ikram M, Rehman S. Enhanced desulfurization characteristics of Cu-KIT-6 for thiophene. Microporous Mesoporous Mater 2014;199:108–16. doi:10.1016/j.micromeso.2014.08.018.

[36] Aslam S, Subhan F, Yan Z, Peng P, Qiao K, Xing W, et al. Facile fabrication of Ni-based KIT-6 for adsorptive desulfurization. Chem Eng J 2016;302:239–48. doi:10.1016/j.cej.2016.05.041.

[37] Varkolu M, Velpula V, Ganji S, Burri DR, Rao Kamaraju SR. Ni nanoparticles supported on mesoporous silica (2D, 3D) architectures: highly efficient catalysts for the hydrocyclization of biomass-derived levulinic acid. RSC Adv 2015;5:57201–10. doi:10.1039/C5RA10857H.

[38] Guo YH, Xia C, Liu BS. Catalytic properties and stability of cubic mesoporous $La_xNi_yO_z$/KIT-6 catalysts for CO_2 reforming of CH_4. Chem Eng J 2014;237:421–9. doi:10.1016/j.cej.2013.09.108.

[39] Grams J, Potrzebowska N, Goscianska J, Michalkiewicz B, Ruppert AM. Mesoporous silicas as supports for Ni catalyst used in cellulose conversion to hydrogen rich gas. Int J Hydrogen Energy 2016;41:8656–67. doi:10.1016/j.ijhydene.2015.12.146.

[40] Prabhu A, Kumaresan L, Palanichamy M, Murugesan V. Synthesis and characterization of aluminium incorporated mesoporous KIT-6: Efficient catalyst for acylation of phenol. Appl Catal A Gen 2009;360:59–65. doi:10.1016/j.apcata.2009.03.004.

[41] Dinari M, Mohammadnezhad G, Nabiyan A. Preparation and characterization of nanocomposite materials based on polyamide-6 and modified ordered mesoporous silica KIT-6. J Appl Polym Sci 2016;133:1–6. doi:10.1002/app.43098.

[42]   Saikia L, Srinivas D, Ratnasamy P. Chemo-, regio- and stereo-selective aerial oxidation of limonene to the endo-1,2-epoxide over Mn(Salen)-sulfonated SBA-15. Appl Catal A Gen 2006;309:144–54. doi:10.1016/j.apcata.2006.05.011.

[43]   Dębek R, Motak M, Duraczyska D, Launay F, Galvez ME, Grzybek T., Da Costa P. Methane dry reforming over hydrotalcite-derived Ni–Mg–Al mixed oxides: the influence of Ni content on catalytic activity, selectivity and stability. Catal Sci Technol 2016;6:6705–15. doi:10.1039/C6CY00906A.
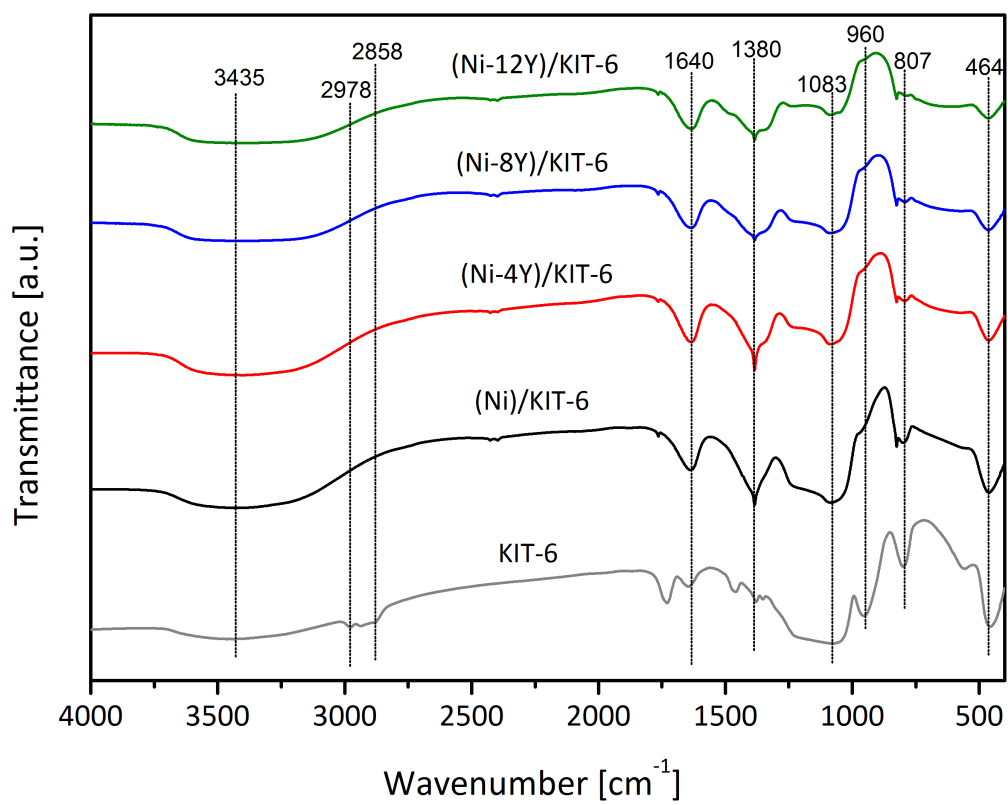
Fig. 1. FT-IR spectra of freshly synthesized KIT-6 support and Ni,Y-modified materials.
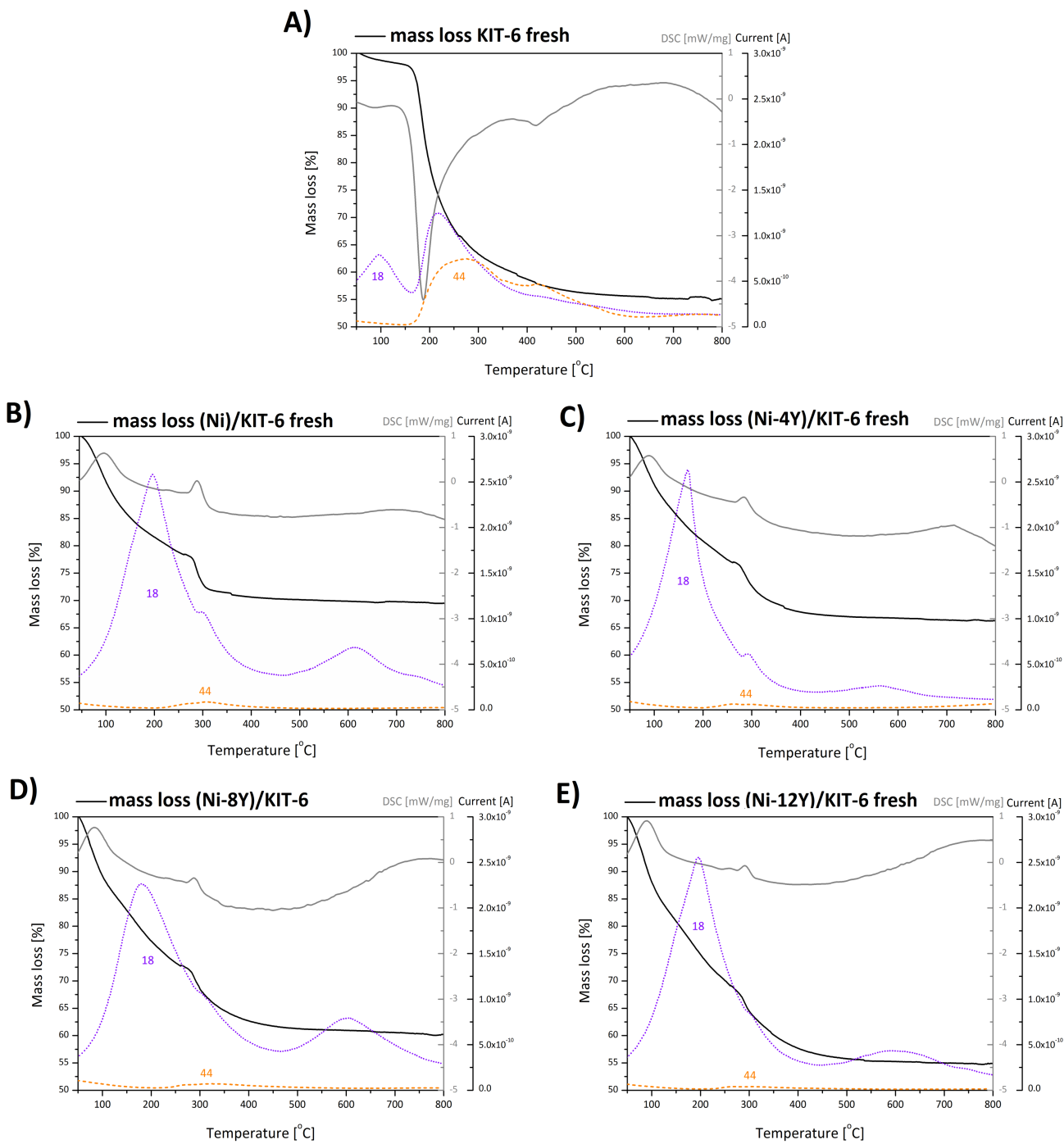
Fig. 2. TGA/DSC-MS curves for KIT-6 freshly synthesized catalysts: KIT-6 (A), (Ni)/KIT-6 (B), (Ni-4Y)/KIT-6 (C), (Ni-8Y)/KIT-6 (D), (Ni-12Y)/KIT-6 (E).

KIT-6 calcined
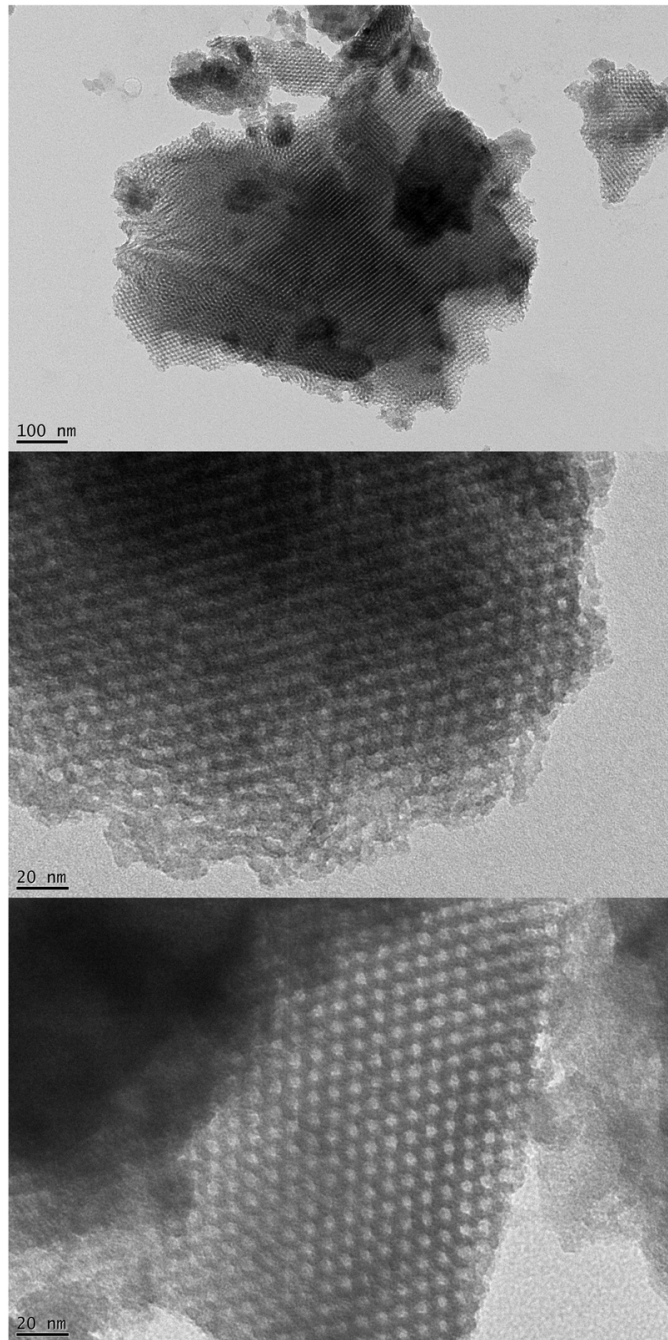
Fig. 3. TEM images of KIT-6 calcined support.
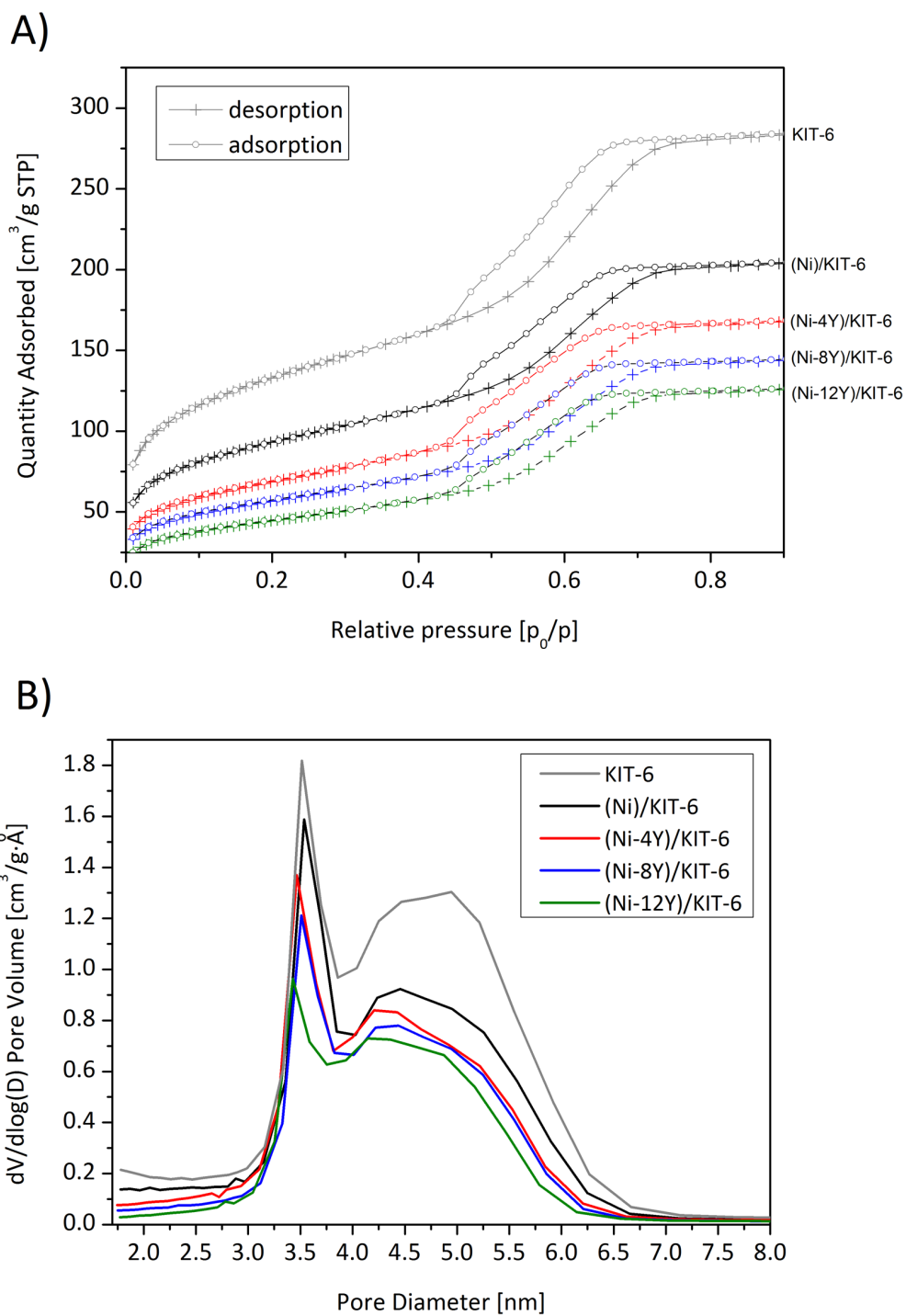
Fig. 4. Isotherms of N_2 adsorption-desorption (A) and distribution of pore diameters (B) for KIT-6 modified materials after calcination at 550°C.
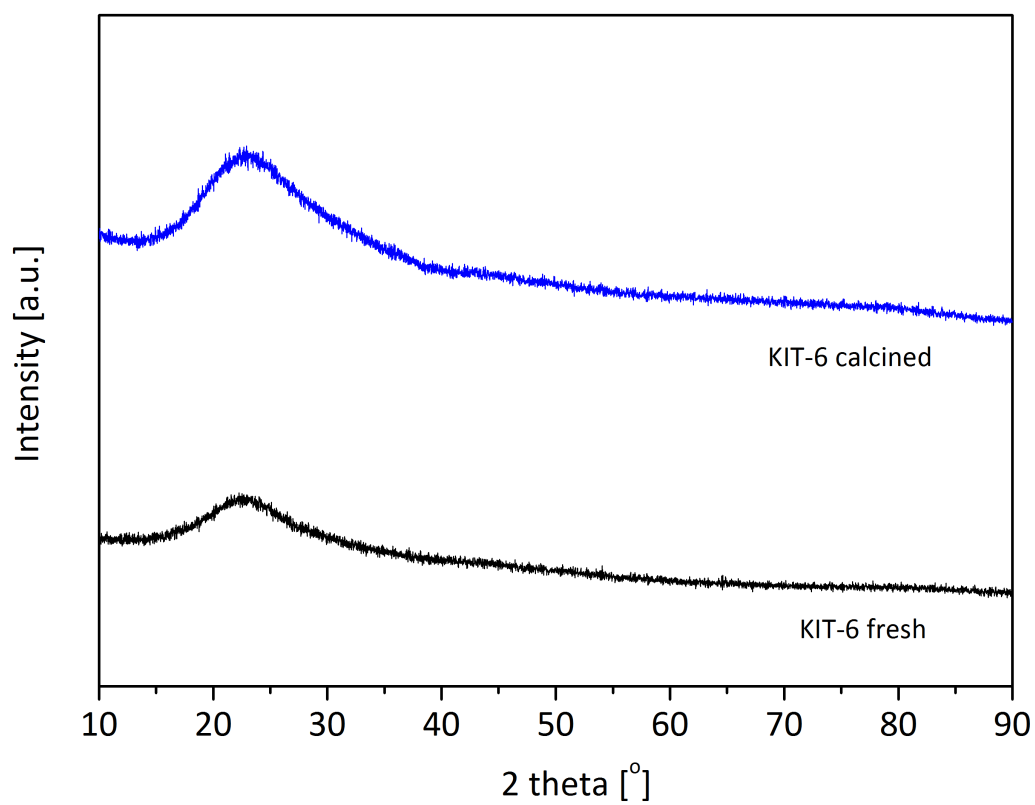
Fig. 5. XRD patterns of freshly synthesized KIT-6 and after calcination at 600ºC for 6h.
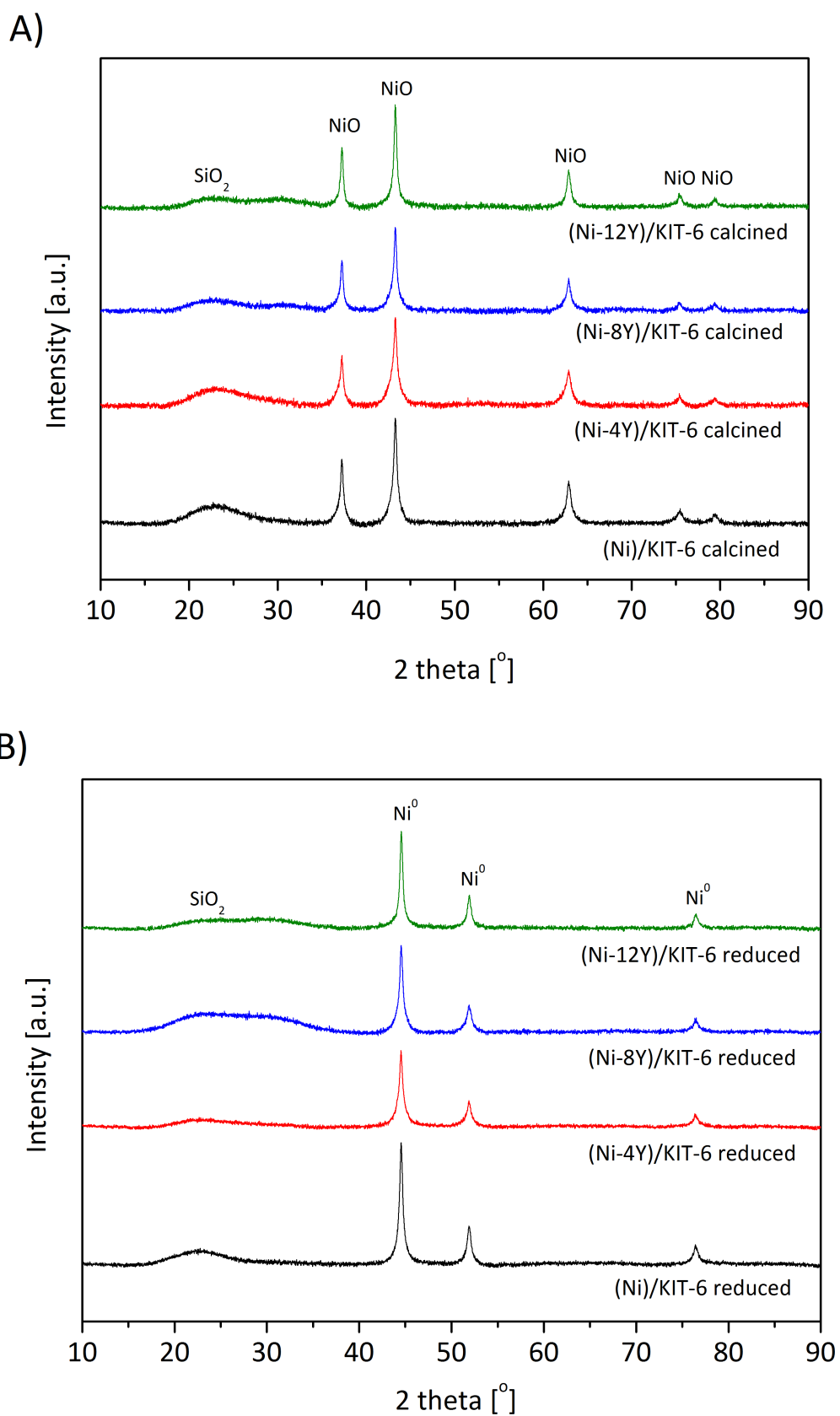
Fig. 6. XRD patterns of Ni,Y-modified KIT-6 supports after calcination at 550°C for 5 h (A) and after reduction in a mixture of 5% H_2/Ar at 750°C for 1h (B).
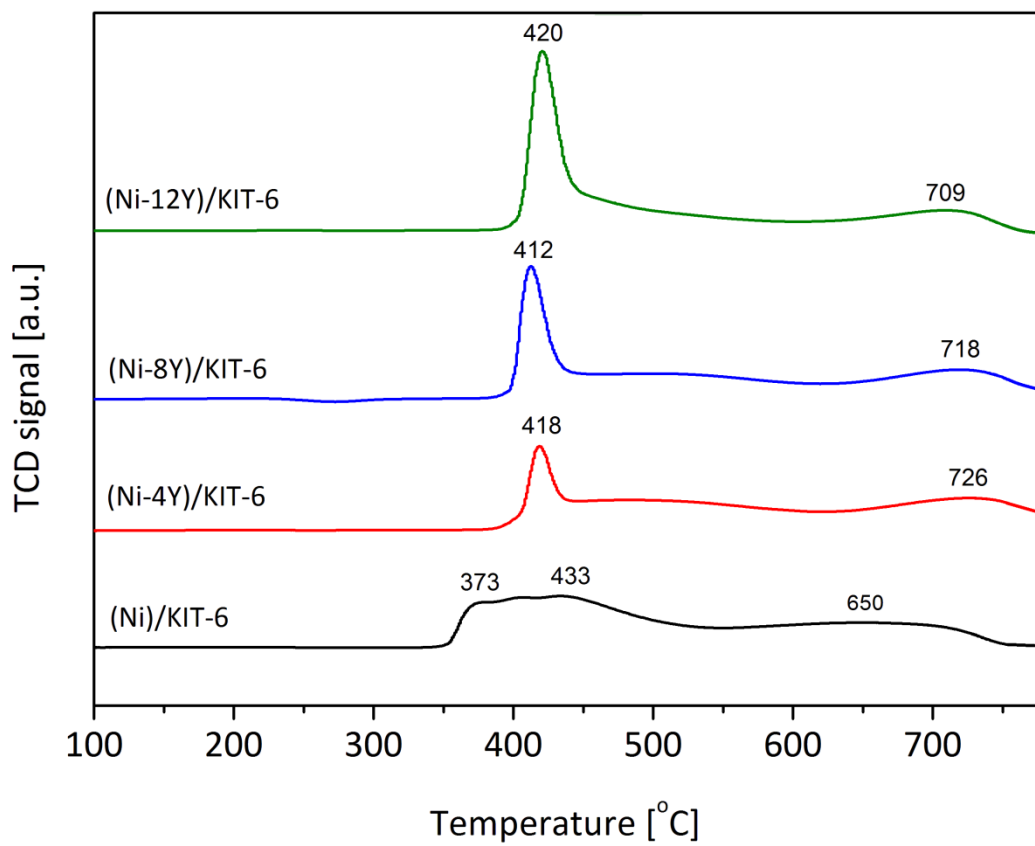
Fig. 7. TPR-H$_2$ of reduced KIT-6 modified samples.

A) (Ni)/KIT-6 reduced
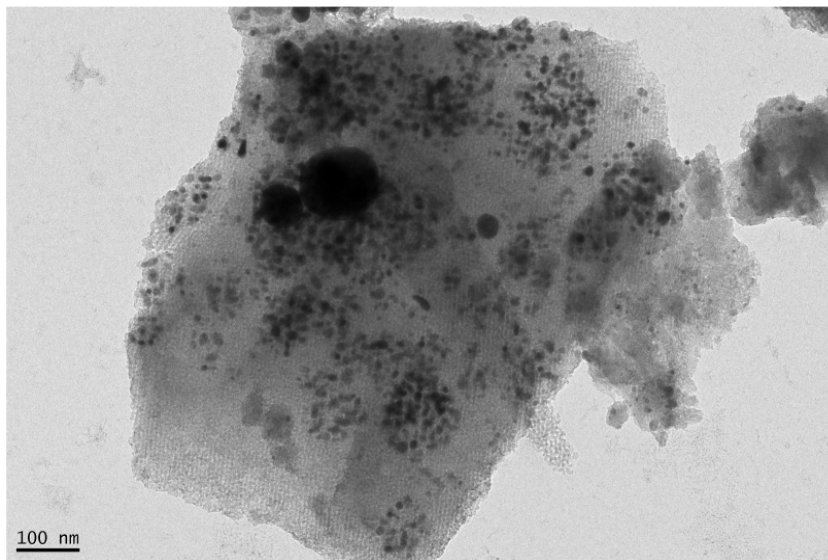
B) (Ni-8Y)/KIT-6 reduced
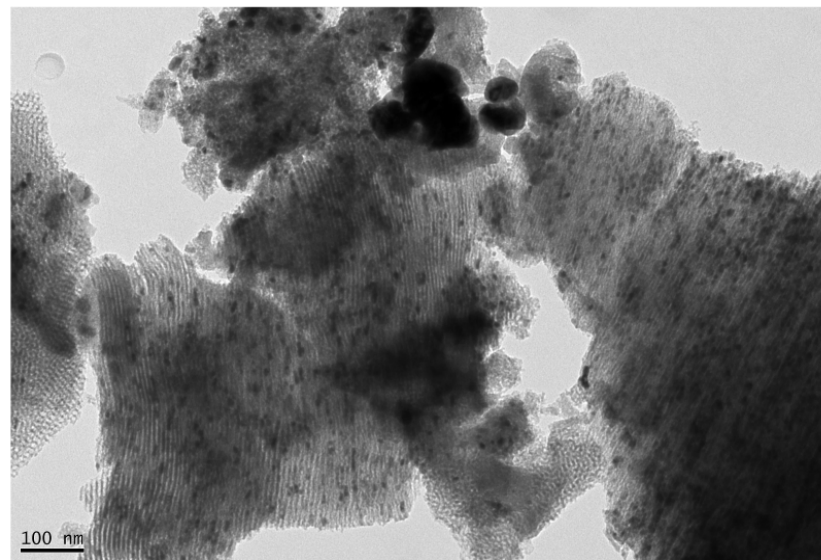
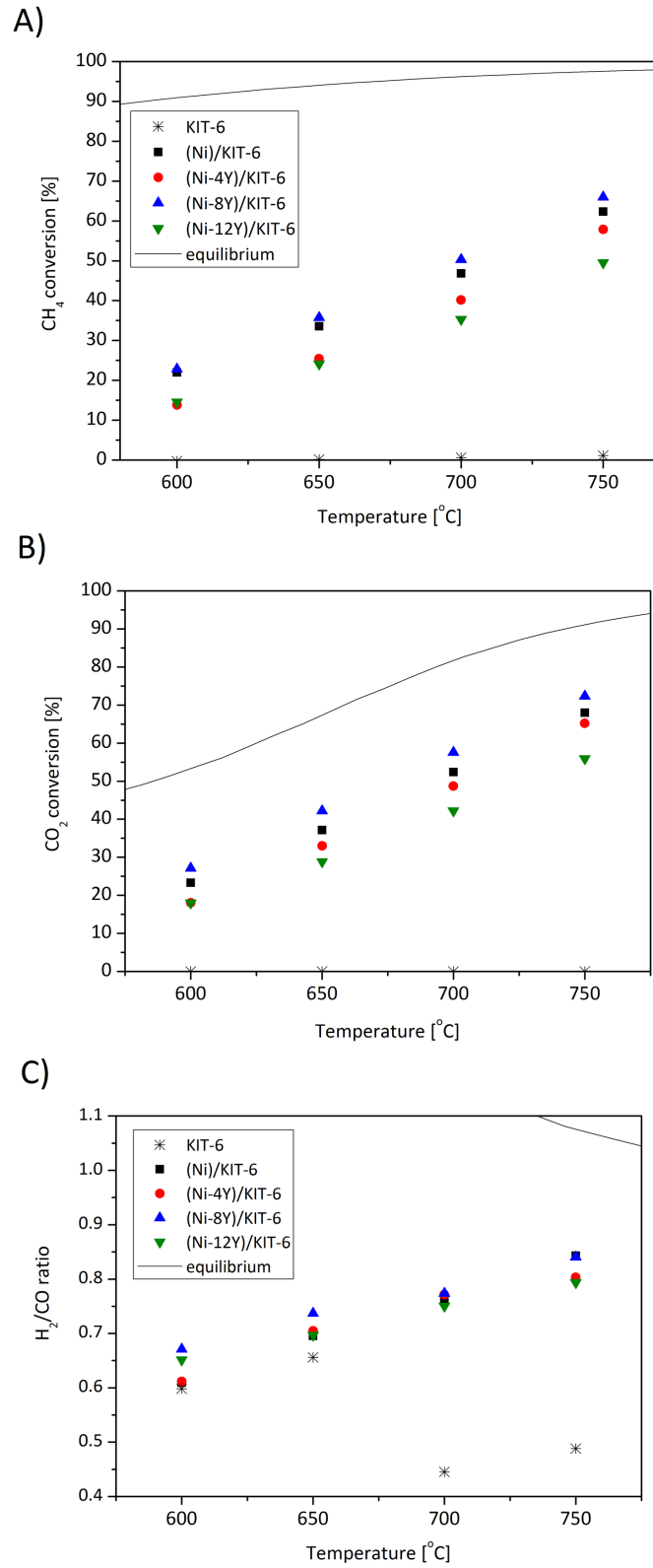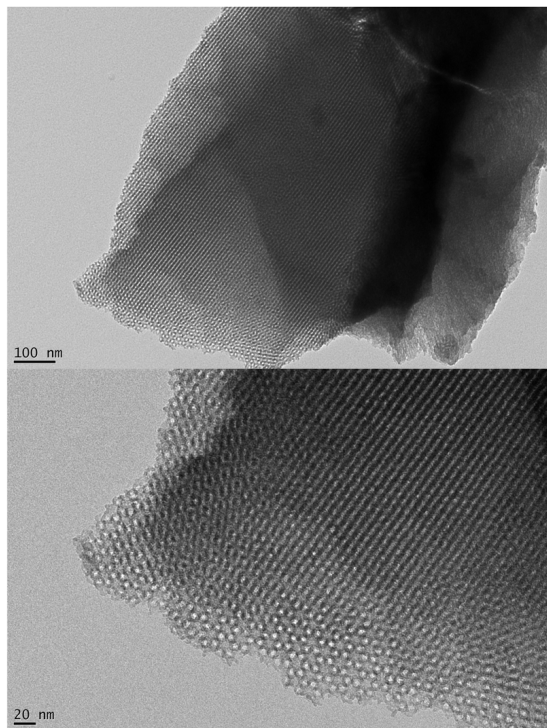Fig. 8. TEM images of (Ni)/KIT-6 (A) and (Ni-8Y)/KIT-6 reduced catalysts.

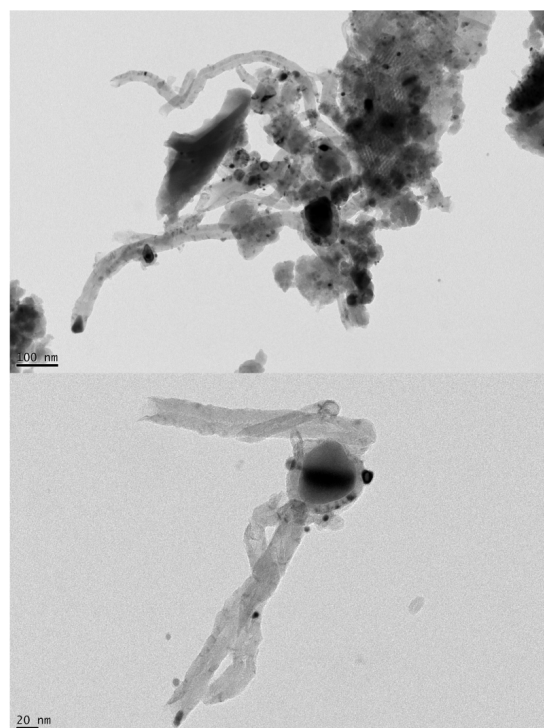Fig 9. Dry methane reforming catalytic tests of KIT-6 modified catalysts (CH₄/CO₂/Ar=1/1/8, GHSV=20,000h⁻¹).

A) KIT-6 spent   B) (Ni)/KIT-6 spent   C) (Ni-8Y)/KIT-6 spent

100 nm

20 nm

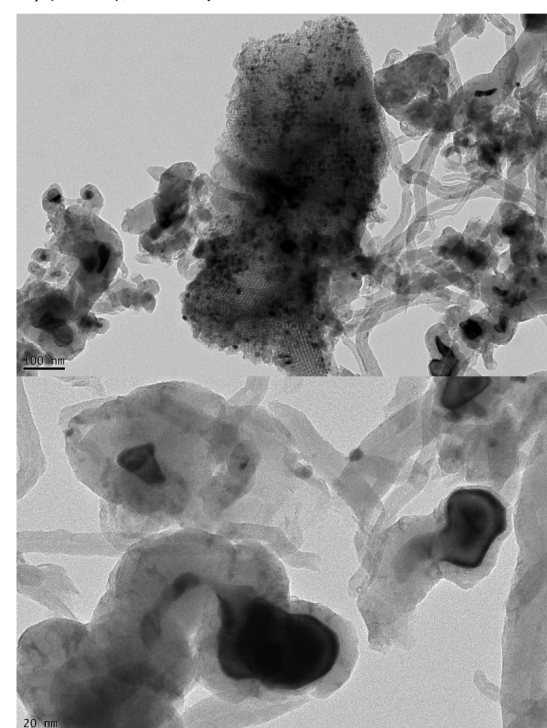100 nm

20 nm

100 nm

20 nm

Fig. 10. TEM micrographs of catalysts after dry methane reforming KIT-6 (A), (Ni)/KIT-6 (B), (Ni-8Y)/KIT-6 (C).
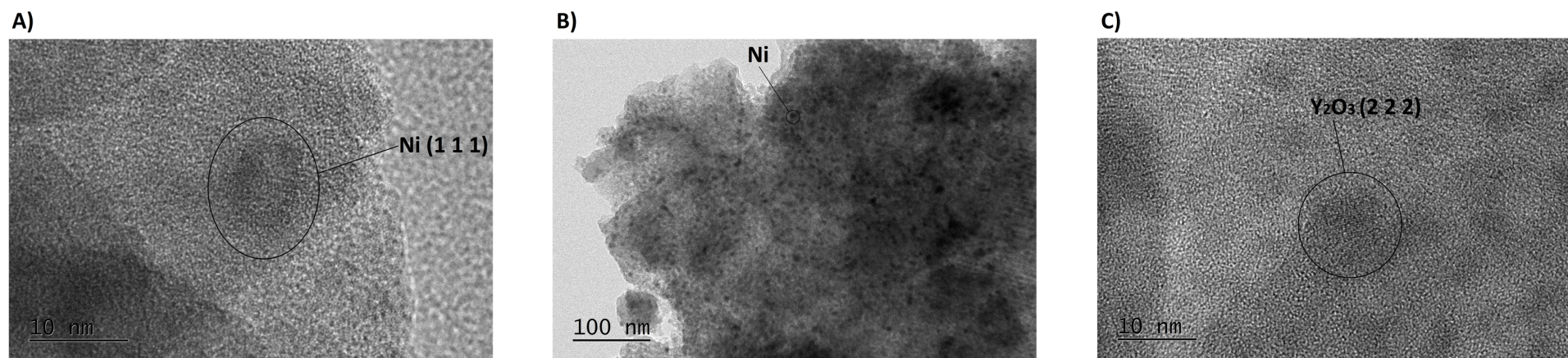
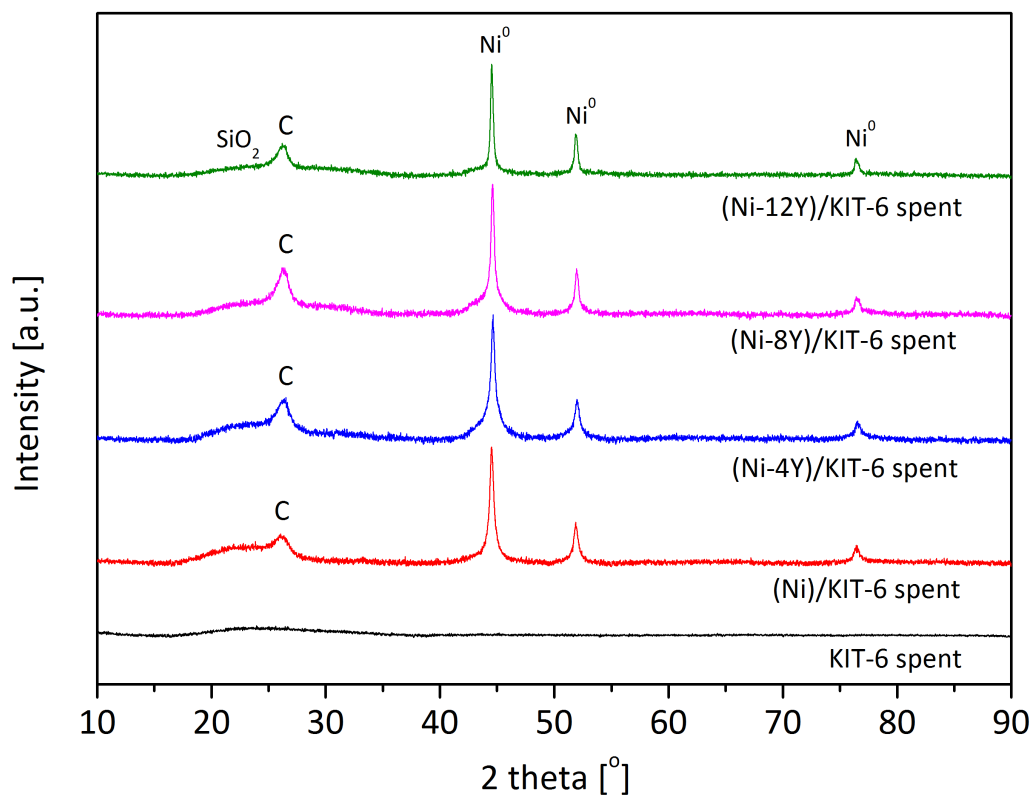Fig. 11. HRTEM micrographs of (Ni-8Y)/KIT-6 catalyst after dry methane reforming.

Fig. 12. XRD patterns of spent catalysts KIT-6, (Ni)/KIT-6, (Ni-4Y)/KIT-6, (Ni-8Y)/KIT-6, (Ni-12Y)/KIT-6.

Table 1 Properties of KIT-6 supported catalysts. The numbers in brackets refer to nominal values.

Catalyst	Elemental composition			Y/Si molar ratio	Textural properties of calcined samples			Textural properties of reduced samples		
	Si [wt. %]	Ni [wt. %]	Y [wt. %]		S_{BET}[1] [m^2/g]	V_p[2] [cm^3/g]	d_p[3] [nm]	S_{BET}[1] [m^2/g]	V_p[2] [cm^3/g]	d_p[3] [nm]
KIT-6	97	-	-	-	456	0.5	4.0	-	-	-
(Ni)/KIT-6	89	7 (12)	-	-	322	0.3	3.9	287	0.3	3.9
(Ni-4Y)/KIT-6	85	8 (12)	2 (4)	0.02	241	0.3	4.0	239	0.2	3.9
(Ni-8Y)/KIT-6	79	9 (12)	4 (8)	0.05	199	0.2	4.0	189	0.2	4.1
(Ni-12Y)/KIT-6	78	10 (12)	7 (12)	0.09	158	0.2	4.1	139	0.2	4.1

[1] specific surface area calculated from the BET equation,

[2] pore volumes derived from BJH desorption method,

[3] average pore size distribution obtained from BJH desorption method.

Table 2 Nickel crystal size (from XRD and TEM analysis) and reducibility (TPR-H_2).

Catalyst	Ni^o crystal size from XRD analysis		Average Ni^o crystal size TEM analysis				Reducibility		
	Reduced catalysts [nm]	Spent catalysts [nm]	Reduced catalysts [nm]		Spent catalysts [nm]		H_2 consumption [μmol H_2/g]		
			Inside pores	External surface	Inside pores	Extrenal surface	I type bulk NiO	II type NiO inside pores	I type/ (I type + II type)
KIT-6	np	np	nd	nd	nd	nd	np	np	np
(Ni)/KIT-6	4	5	14	66	11	26	0.030	0.016	0.35
(Ni-4Y)/KIT-6	6	9	nd	nd	nd	nd	0.031	0.015	0.32
(Ni-8Y)/KIT-6	7	18	9	83	8	51	0.034	0.008	0.19
(Ni-12Y)/KIT-6	13	23	nd	nd	nd	nd	0.052	0.011	0.17